Development of Neutron Interferometer Using Multilayer Mirrors and Measurements of Neutron-Nuclear Scattering Length with Pulsed Neutron Source

Takuhiro Fujiie[1,2,*] Masahiro Hino,[3] Takuya Hosobata,[2] Go Ichikawa,[4,5] Masaaki Kitaguchi,[1,4,6] Kenji Mishima,[4,5] Yoshichika Seki,[7] Hirohiko M. Shimizu,[1,4] and Yutaka Yamagata[2]

[1]*Department of Physics, Nagoya University, Furocho Chikusa, Nagoya 464-8602, Aichi, Japan*
[2]*RIKEN Center for Advanced Photonics, Hirosawa 2-1, Wako 351-0198, Saitama, Japan*
[3]*Institute for Integrated Radiation and Nuclear Science, Kyoto University,*
2, Asashiro-Nishi, Kumatori, Sennan-gun 590-0494, Osaka, Japan
[4]*High Energy Accelerator Research Organization, Tokai, Ibaraki 319-1106, Japan*
[5]*J-PARC Center, 2-4 Tokai, Ibaraki 319-1195, Japan*
[6]*Kobayashi-Maskawa Institute, Nagoya University, Furocho Chikusa, Nagoya 464-8602, Aichi, Japan*
[7]*Institute of Multidisciplinary Research for Advanced Materials, Tohoku University,*
Katahira 2-1-1, Aoba-ku, Sendai 980-8577, Japan

This study entailed the successful deployment of a novel neutron interferometer that utilizes multilayer mirrors. The apparatus facilitates a precise evaluation of the wavelength dependence of interference fringes utilizing a pulsed neutron source. Our interferometer achieved an impressive precision of 0.02 rad within a 20-min recording time. Compared to systems using silicon crystals, the measurement sensitivity was maintained even when using a simplified disturbance suppressor. By segregating beam paths entirely, we achieved successful measurements of neutron-nuclear scattering lengths across various samples. The values measured for Si, Al, and Ti were in agreement with those found in the literature, while V showed a disparity of 45%. This discrepancy may be attributable to impurities encountered in previous investigations. The accuracy of measurements can be enhanced further by mitigating systematic uncertainties that are associated with neutron wavelength, sample impurity, and thickness. This novel neutron interferometer enables us to measure fundamental parameters, such as the neutron-nuclear scattering length of materials, with a precision that surpasses that of conventional interferometers.

Neutron interferometers, which are characterized by a neutron wave that is divided into two paths and then merged while sustaining its coherence [1], are used for the precise measurement of neutron-related interactions [2]. Specifically, the Mach-Zehnder-type neutron interferometer, which utilizes diffraction from a Si single crystal and was first demonstrated by Rauch in 1974 [3], has been broadly applied in a variety of physics experiments. These include measurements of neutron-nuclear scattering length [4–6], demonstrations of classical physics with elementary particles [7,8], validations of quantum mechanics [9–14], and investigations of exotic interactions as predicted by new physics [15,16]. Recent proposals for experiments using neutron interferometers to probe new physics underscore their continuing significance [17–22].

The sensitivity of the interactions measured is directly proportional to the neutron wavelength and the interaction length. However, neutron interferometers that use Si crystal are limited by the lattice constant in terms of the available neutron wavelengths and are also size constrained by the dimensions of the ingot [1]. Progress is being made in developing neutron interferometers capable of high-sensitivity measurements to overcome these limitations [23–25]. Among them, Jamin-type neutron interferometers, which use neutron mirrors to reflect neutrons through an artificially fabricated multilayer structure to separate and recombine neutron paths [26–28], offer a significant advantage. The multilayer structure allows for the selection of neutron wavelengths based on specific design parameters [29].

We introduce a novel neutron interferometer, integrating unpolarized neutron mirrors with a pulsed neutron source capable of identifying the wavelength from the time of flight (TOF) at J-PARC. The interferometer concurrently measures phase shifts at diverse wavelengths, bestowing a significant statistical advantage. It also enables tracking and rectification of time-varying disturbances beyond the pulse interval [30], thus circumventing the issues encountered by conventional systems using multilayer mirrors [31]. This Letter accentuates that the developed interferometer achieved phase shift measurements with sensitivity comparable to systems employing Si crystals, even with simple disturbance suppressors. We also successfully conducted measurements of the neutron-nuclear scattering lengths for
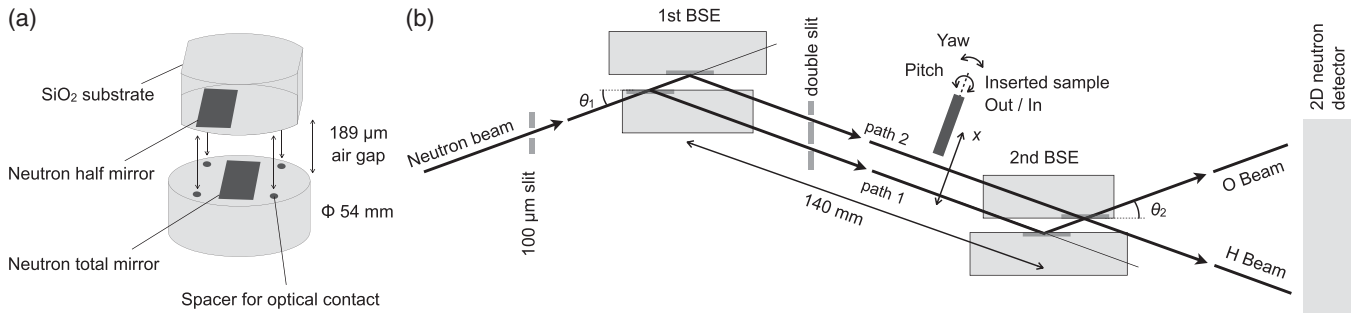
FIG. 1. Illustration drawing of the design of our interferometer. (a) BSE with neutron mirror deposited. (b) Assembly of the interferometer, which is composed of two BSEs. Here, θ_1 and θ_2 signify the incident angles of the neutron wave onto the first and second BSE, respectively. Beam size perpendicular to x was collimated to 12 mm before the first BSE.

several nuclei. This breakthrough underscores a crucial advancement in neutron interferometry, enhancing sensitivity for fundamental physics involving neutrons.

The experiment was conducted at the low-divergence branch of BL05 (NOP) within the Materials and Life Science Experimental Facility at J-PARC [32–35]. Pulsed neutrons, generated through the spallation reaction at a repetition frequency of 25 Hz, were moderated by a liquid hydrogen moderator and directed to the experimental setup via a neutron mirror bender, a four-blade slit, and a vacuum guide tube. The beam power sustained during the experiments was 620 kW.

Our interferometer comprised two beam-splitting etalons (BSEs) [Fig. 1(a)] that split neutron waves into two parallel paths and later recombined them [Fig. 1(b)]. The BSEs were designed with half and total reflection mirrors separated by an air gap of $D = 189$ μm [28,36]. The mirrors, deposited on a flat SiO_2 substrate, were bonded by optical contact to maintain parallelism. The parallelism was preserved at approximately 30 nm, roughly in the range of typical transverse coherence length of the neutrons in this setup. The neutron mirror, made from a Ni and Ti multilayer structure, can reflect momentum transfers in the range of $0.232 < Q < 0.292$ nm^{-1} [37]. The BSEs were positioned at an incident angle θ_1 of 1.05° with respect to the neutrons, with the centers of the two BSEs distanced 140 mm apart. The neutron wave, having been divided into two paths, passed through a double slit situated 60 mm away from the center of the first BSE before being redirected toward the second BSE. This double-slit configuration consisted of two grooves, each 130 μm wide, separated by a center-to-center distance of 326 μm. This design was optimized based on the incident angle and refraction characteristics of the BSEs. The interference pattern of the neutron waves was detected by a neutron detector equipped with time and two-dimensional position detection capabilities [38]. The detector was placed 400 mm away from the center of the second BSE. To minimize external disturbances, the interferometer and sample insertion assembly were placed on an active vibration isolator and maintained at a stable temperature

of 23 °C inside a thermostatic chamber. Over 9.2 h, the temperature's standard deviation remained at 0.035 K.

A Cd mask, 1 mm in thickness, was systematically traversed across the two beam paths located between the BSEs to quantify the beam profile. The mask sequentially shielded neutron waves by scanning in the x direction using a sample insertion assembly. The neutron intensities pertaining to the O and H beams, along with their differentials, are shown in Fig. 2. The distinct staircase pattern in the neutron intensities indicates the complete bifurcation of neutrons into two separate paths by the first BSE and the double slit. A double Gaussian fitting applied to the derivative of the neutron intensity confirmed the path separation to be 326 μm, consistent with design specifications.

The relative angle $\delta\theta = \theta_2 - \theta_1$ could be adjusted with a resolution of 6 μrad using a micrometer affixed to the second BSE. The parallel alignment of the second BSE was achieved using an autocollimator with an accuracy of 3 μrad. After alignment, periodic intensity distributions were observed in the TOF region from 35 to 50 ms [refer to Fig. 3(a)]. The absence of oscillation patterns when a single path was obstructed by a Cd mask indicates that these oscillations were due to the interference of neutron waves from the two paths.
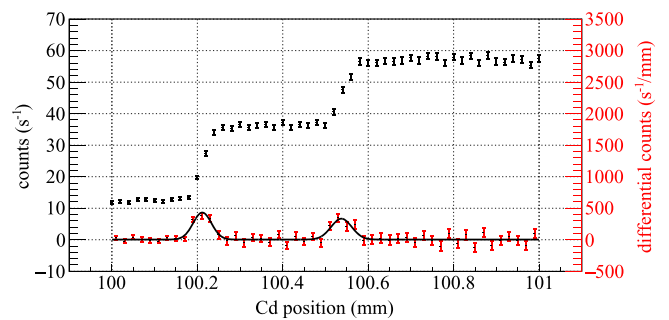

FIG. 2. Overall neutron intensity of O and H beams in relation to the position of the Cd mask (black) and the corresponding differential intensity (red) that has been fit using a double Gaussian model.
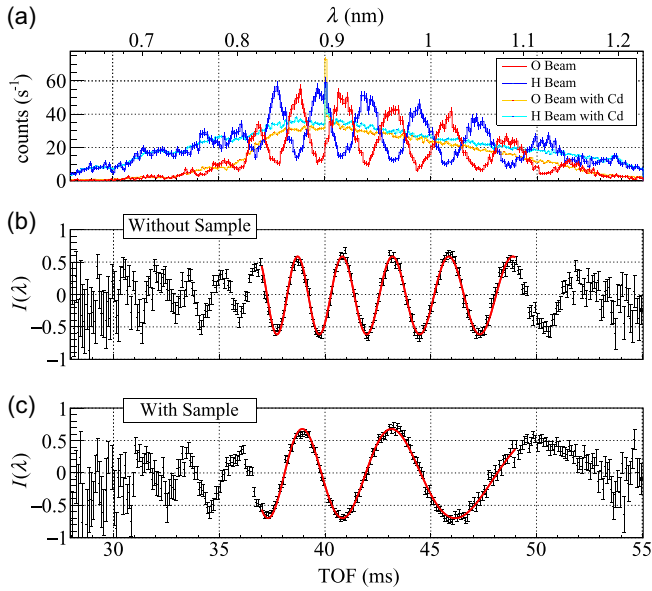
FIG. 3. TOF dependency of the measured interference fringes. (a) TOF spectra of neutron intensity in the O and H beams. The spectra of pale color (orange and cyan lines) indicate the incoherent sum of both interferometer paths, obtained by blocking one or the other path with Cd and summing up both contributions. (b) Interference fringes obtained from the above spectrum. (c) Variation in the interference fringes prompted by the insertion of a Si sample. The measurement time attributed to these fringes was 10 min. For each spectrum, background readings were subtracted.

Interference fringes were calculated from the following equation:

$$I(\lambda) = \frac{I_O/I_{O_{Cd}} - I_H/I_{H_{Cd}}}{I_O/I_{O_{Cd}} + I_H/I_{H_{Cd}}}, \tag{1}$$

where I_O and I_H represent the measured TOF spectra of O and H beams, respectively, while $I_{O_{Cd}}$ and $I_{H_{Cd}}$ symbolize the spectra with a single path blocked by the Cd mask. Any prompt event stemming from proton collision with the mercury target within the $40 < \text{TOF} < 40.1$ ms region was deliberately excluded from the analysis. The interference fringe, normalized by Eq. (1), is shown in Fig. 3(b). This interference fringe can be fitted by the following equation:

$$I(\lambda) = A \cos\left(\frac{P_L}{\lambda} + P_R\lambda - P_S\lambda\right) + B, \tag{2}$$

where λ denotes the neutron wavelength (the derivation is provided in Supplemental Material [39]). The initial term in the cosine function signifies the geometric optical length difference, $P_L = 4\pi D\delta\theta$, between the two paths, where D is the BSE's air gap. The second term, $P_R = -4\pi D\delta\theta m U/(h^2\theta_1^2)$, denotes the path difference multiplied by the refractive index in SiO_2 of the BSE.

Here, U represents the Fermi pseudopotential of SiO_2, m is the neutron mass, and h is Planck's constant. The third term, $P_S = Nb_c t$, corresponds to the interaction with the inserted sample, where N is the atomic number density, b_c is the neutron-nuclear scattering length, and t is the thickness. The phase shifts, depicted as the third term, are directly linked to the sensitivity of the measured interactions. The visibility, represented by A, typically approximated 60%. The effects of discrepancies between paths, such as differences in mirror reflectivity and neutron absorption by the sample, appear in the B term. Typically, it was about 3%, but this does not affect the determination of the scattering length. The fitting region was identified as the TOF range from 37 to 49 ms, where the interference fringes were clearly discernible.

Figure 3(c) shows the interference fringe produced upon inserting a 0.3-mm-thick Si sample into one of the paths. A significant phase change occurred from the configuration without the sample. The uncertainty in the measured phase shift caused by the sample was obtained to be 0.02 rad per 20 min. This sensitivity exceeded that measured by NIST (0.31 rad per min) [31] by a factor of 3 and was comparable to that measured by ILL (0.08 rad per min) [11]. Contrary to the Si interferometer's requirement for a 5 mK temperature accuracy [43], which is an order of magnitude more stringent, the precision in phase determination is improved. The time fluctuation of P_S was 3×10^{-3} rad over a 20-min period, a value 4 orders of magnitude smaller than the phase shift caused by the Si sample, approximately 60 rad. These results validate the interferometer's effectiveness within a simple thermostatic chamber, indicating its robust stability during extended measurement periods.

The phase of the fringes can be modified by adjusting $\delta\theta$ using the micrometer affixed to the second BSE. The alteration in P_L relative to $\delta\theta$ was recorded as $P_L/\delta\theta = 2.13 \pm 0.01$ nm/µrad [Fig. 4(a)], approximately
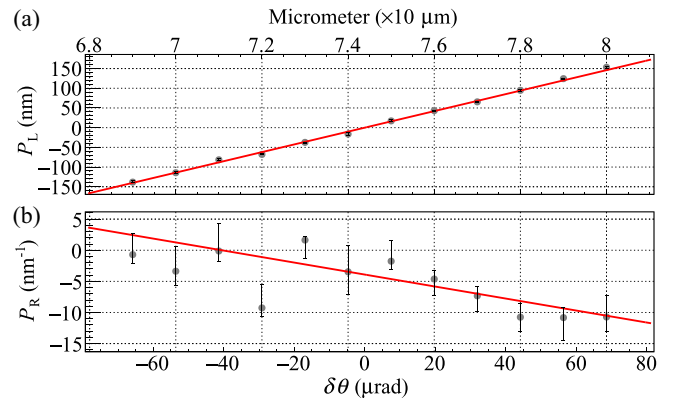

FIG. 4. Relationship of $\delta\theta$ with (a) P_L and (b) P_R, characterized by a linear function. The conversion factor between the micrometer value and $\delta\theta$ is established as 12.22 µrad/µm. The baseline value for $\delta\theta$ was determined through the fitting process applied to P_L.

TABLE I.   Each sample yielded measured b_c. Reference values of b_c^{ref} were taken from Sears [45].

Sample	t (mm)	Purity (wt %)	Statistics uncertainties	Systematics uncertainties	b_c (fm)	b_c/b_c^{ref}
Si[a]	0.287 ± 0.001	99.999+	9.2×10^{-5}	6.7×10^{-3}	4.060 ± 0.027	0.978 ± 0.007
Ti	0.100 ± 0.002	99.5+	4.4×10^{-4}	1.8×10^{-2}	-3.477 ± 0.062	1.011 ± 0.018
	0.204 ± 0.004	99.5+	2.0×10^{-4}	1.9×10^{-2}	-3.386 ± 0.064	0.985 ± 0.019
Al	0.103 ± 0.001	99+	6.0×10^{-4}	1.5×10^{-2}	3.408 ± 0.050	0.988 ± 0.015
	0.287 ± 0.002	99+	5.3×10^{-5}	7.8×10^{-3}	3.423 ± 0.027	0.992 ± 0.008
	0.961 ± 0.001	99+	4.1×10^{-5}	5.7×10^{-3}	3.466 ± 0.020	1.005 ± 0.006
V	0.316 ± 0.001	99.7+[b]	3.9×10^{-4}	6.8×10^{-3}	-0.522 ± 0.004	1.364 ± 0.010
	0.314 ± 0.002	99.7+[b]	6.1×10^{-4}	7.2×10^{-3}	-0.520 ± 0.004	1.361 ± 0.011
V averaged	$\cdots$	$\cdots$	$\cdots$	$\cdots$	-0.521 ± 0.003	1.363 ± 0.008
V-Ni alloy[c]	0.315 ± 0.006	V : Ni = 94.582 : 5.32[b]	3.1×10^{-3}	1.8×10^{-2}	-0.062 ± 0.001	-0.528 ± 0.010

[a]N-type wafer.
[b]The contaminations are summarized in Supplemental Material [39].
[c]Fabricated by Taiyo Koko Co., Ltd.

10% less than the theoretical value of 2.38 nm/μrad. The change in P_R was estimated to be $P_R/\delta\theta = -0.096 \pm 0.020$ nm^{-1}/μrad [Fig. 4(b)], nearly a quarter of the theoretical value of -0.39 nm^{-1}/μrad. These deviations are speculated to arise from geometric inaccuracies in the BSEs or potential misalignment of the micrometer. Importantly, these effects can be compensated by calculating phase shifts in the presence and absence of the sample.

To demonstrate our interferometer's capabilities, we conducted experiments to determine neutron-nucleus scattering lengths. We selected Si and Al as representative nuclei, Ti and V as nuclei with negative b_c values, and V-Ni alloy as nuclei with near-zero b_c. The V-Ni alloy is frequently employed in neutron scattering experiments as sample containers to prevent Bragg scatterings [40]. For accurate results, samples were precisely adjusted to minimize phase shifts in the interference fringes using three-axis stages [Fig. 1(b)]. Measurements of P_S were conducted with and without the sample for 5 min each to eliminate disturbances. This process was repeated over several hours for each sample (see Supplemental Material [39] for further details).

The obtained b_c values, along with their systematic and statistical uncertainties and the sample thicknesses, are listed in Table I. The systematic uncertainties considered are detailed in Supplemental Material [39], including Refs. [1,41]. The values for Si, Al, and Ti were consistent with the literature values, accurate to within 2.2%. However, the results were generally smaller compared to the literature values, potentially due to systematic discrepancies between the TOF method-derived wavelengths and the true values [44]. Notably, the statistical uncertainty was 2 orders of magnitude less than the systematic uncertainty. Future work to enhance b_c determination accuracy should prioritize minimizing systematic uncertainties arising from sample conditions.

In contrast to the aforementioned samples, the results for the V and V-Ni alloy samples deviated significantly from their respective literature values. We conducted elemental analyses on the V and V-Ni alloy samples used in the measurements to investigate the underlying cause of this discrepancy. However, no significant impurities were identified. A comprehensive summary of all measured impurities can be found in Supplemental Material [39] including Refs. [40,42]. To eliminate uncertainty arising from the neutron wavelength of the pulse source, we determined the b_c of V relative to Si using both V and V-Ni alloy samples. The effects of measured impurities were also eliminated. The derived b_c values for V were -0.555 ± 0.003 fm from the V sample and -0.559 ± 0.005 fm from the V-Ni alloy sample. We used the b_c values of Si as 4.1491 ± 0.0010 fm and Ni as 10.3 ± 0.1 fm [45]. Both values of V were found to be in agreement but deviated by 45% from the NIST-recommended value of -0.3824 ± 0.0012 fm [46]. Supporting this finding, a previous report suggested that the minimization of the Bragg peak required a higher amount of Ni in the V-Ni alloy compared to the NIST database [40].

In conclusion, we have developed a neutron interferometer utilizing multilayer mirrors. The successful operation of our interferometer with pulsed neutrons at J-PARC yielded a visibility of 60%. Significantly, our interferometer demonstrated exceptional precision in phase determination, achieving an accuracy of 0.02 rad within a 20-min interval. Furthermore, our interferometer utilized a neutron wavelength of approximately 0.9 nm, providing enhanced sensitivity for specific applications compared to Si interferometers using 0.19–0.44 nm. The phase drift over time measured in our interferometer was 4 orders of magnitude smaller than the phase shift induced by a 0.3-mm-thick Si sample. Our interferometer demonstrates robustness against fluctuations, making it highly reliable. By introducing samples into one of the paths, we measured

the b_c values for Si, Al, Ti, V, and V-Ni alloy. These measurements exhibited agreement with literature values within an accuracy of 2.2%, except for vanadium, which requires further investigation to determine if impurities in the V sample contributed to the observed discrepancy. These findings indicate that the phase shift introduced by the inserted samples was accurately captured.

The statistical uncertainty associated with the measured phase shift was significantly smaller, up to 2 orders of magnitude, than the systematic uncertainty. This emphasizes the potential for highly sensitive measurements. To mitigate uncertainty in wavelength determination, two approaches can be employed: conducting relative measurements to Si or performing precise wavelength measurements. Furthermore, enhancing the sensitivity of b_c can be achieved by using thicker samples with reduced impurities. The systematic uncertainty arising from nonuniform sample thickness can be addressed through ultrahigh-precision machining technology [47,48].

Replacing the current multilayers with supermirrors and reflecting neutrons within the optimal wavelength range of 0.2–0.8 nm at J-PARC BL05 can increase statistics by a factor of 20. This improvement would render the two-pathway separation interferometer nearly as sensitive as grating interferometers [24]. Expanding the BSE's air gap by using a thicker spacer or by independently controlling each mirror could enable the measurement of various interactions, such as the scattering length of gas samples requiring containers of sufficient size [15,16,49]. The utilization of a high-sensitivity neutron interferometer opens up possibilities for a wide range of new physics search experiments [15–22]. The findings of this study represent the initial step toward realizing these experiments.

*fujiie@phi.phys.nagoya-u.ac.jp

[1] H. Rauch and S. A. Werner, *Neutron Interferometry*, 2nd ed. (Oxford, New York, 2015), 10.1093/acprof:oso/9780198712510.001.0001.

[2] S. Sponar, R. I. P. Sedmik, M. Pitschmann, H. Abele, and Y. Hasegawa, Tests of fundamental quantum mechanics and dark interactions with low-energy neutrons, Nat. Rev. Phys. **3**, 309 (2021).

[3] H. Rauch, W. Treimer, and U. Bonse, Test of a single crystal neutron interferometer, Phys. Lett. **47A**, 369 (1974).

[4] S. Hammerschmied, H. Rauch, H. Clerc, and U. Kischko, Measurements of the coherent neutron-tritium scattering length and its relation to the four nucleon problem, Z. Phys. A **302**, 323 (1981).

[5] H. Rauch and D. Tuppinger, New methods for interferometric neutron scattering lengths measurements, Z. Phys. A **322**, 427 (1985).

[6] A. Ioffe, D. L. Jacobson, M. Arif, M. Vrana, S. A. Werner, P. Fischer, G. L. Greene, and F. Mezei, Precision neutron-interferometric measurement of the coherent neutron-scattering length in silicon, Phys. Rev. A **58**, 1475 (1998).

[7] R. Colella, A. W. Overhauser, and S. A. Werner, Observation of gravitationally induced quantum interference, Phys. Rev. Lett. **34**, 1472 (1975).

[8] S. A. Werner, J. L. Staudenmann, and R. Colella, Effect of Earth's rotation on the quantum mechanical phase of the neutron, Phys. Rev. Lett. **42**, 1103 (1979).

[9] H. Rauch, A. Wilfing, W. Bauspiess, and U. Bonse, Precise determination of the 4π-periodicity factor of a spinor wave function, Z. Phys. B Condens. Matter Quanta **29**, 281 (1978).

[10] A. Cimmino, G. I. Opat, A. G. Klein, H. Kaiser, S. A. Werner, M. Arif, and R. Clothier, Observation of the topological Aharonov-Casher phase shift by neutron interferometry, Phys. Rev. Lett. **63**, 380 (1989).

[11] Y. Hasegawa, R. Loidl, G. Badurek, M. Baron, and H. Rauch, Violation of a Bell-like inequality in single-neutron interferometry, Nature (London) **425**, 45 (2003).

[12] D. A. Pushin, M. G. Huber, M. Arif, and D. G. Cory, Experimental realization of decoherence-free subspace in neutron interferometry, Phys. Rev. Lett. **107**, 150401 (2011).

[13] C. W. Clark, R. Barankov, M. G. Huber, M. Arif, D. G. Cory, and D. A. Pushin, Controlling neutron orbital angular momentum, Nature (London) **525**, 504 (2015).

[14] T. Denkmayr, J. Dressel, H. Geppert-Kleinrath, Y. Hasegawa, and S. Sponar, Weak values from strong interactions in neutron interferometry, Physica (Amsterdam) **551B**, 339 (2018).

[15] H. Lemmel, P. Brax, A. N. Ivanov, T. Jenke, G. Pignol, M. Pitschmann, T. Potocar, M. Wellenzohn, M. Zawisky, and H. Abele, Neutron interferometry constrains dark energy chameleon fields, Phys. Lett. B **743**, 310 (2015).

[16] K. Li, M. Arif, D. G. Cory, R. Haun, B. Heacock, M. G. Huber, J. Nsofini, D. A. Pushin, P. Saggu, D. Sarenac, C. B. Shahi, V. Skavysh, W. M. Snow, and A. R. Young, Neutron limit on the strongly-coupled chameleon field, Phys. Rev. D **93**, 062001 (2016).

[17] H. Okawara, K. Yamada, and H. Asada, Possible daily and seasonal variations in quantum interference induced by Chern-Simons gravity, Phys. Rev. Lett. **109**, 231101 (2012).

[18] C. J. Riedel, Direct detection of classically undetectable dark matter through quantum decoherence, Phys. Rev. D **88,** 116005 (2013).

[19] C. J. Riedel and I. Yavin, Decoherence as a way to measure extremely soft collisions with dark matter, Phys. Rev. D **96,** 023007 (2017).

[20] T. A. Brun and L. Mlodinow, Detecting discrete spacetime via matter interferometry, Phys. Rev. D **99,** 015012 (2019).

[21] J. M. Rocha and F. Dahia, Neutron interferometry and tests of short-range modifications of gravity, Phys. Rev. D **103,** 124014 (2021).

[22] S. Iwaguchi, A. Nishizawa, Y. Chen, Y. Kawasaki, M. Kitaguchi, T. Morimoto, T. Ishikawa, B. Wu, I. Watanabe, R. Shimizu, H. Shimizu, Y. Michimura, and S. Kawamura, Displacement-noise-free neutron interferometer for gravitational wave detection using a single Mach-Zehnder configuration, Phys. Lett. A **441,** 128150 (2022).

[23] D. A. Pushin, M. Arif, and D. G. Cory, Decoherence-free neutron interferometry, Phys. Rev. A **79,** 053635 (2009).

[24] D. Sarenac, D. A. Pushin, M. G. Huber, D. S. Hussey, H. Miao, M. Arif, D. G. Cory, A. D. Cronin, B. Heacock, D. L. Jacobson, J. M. LaManna, and H. Wen, Three phase-grating Moiré neutron interferometer for large interferometer area applications, Phys. Rev. Lett. **120,** 113201 (2018).

[25] H. Lemmel, M. Jentschel, H. Abele, F. Lafont, B. Guerard, C. P. Sasso, G. Mana, and E. Massa, Neutron interference from a split-crystal interferometer, J. Appl. Crystallogr. **55,** 870 (2022).

[26] H. Funahashi, T. Ebisawa, T. Haseyama, M. Hino, A. Masaike, Y. Otake, T. Tabaru, and S. Tasaki, Interferometer for cold neutrons using multilayer mirrors, Phys. Rev. A **54,** 649 (1996).

[27] M. Kitaguchi, Cold-neutron interferometry using beam splitting etalons, Ph.D. thesis, Kyoto University, 2004, 10.14989/doctor.k11047.

[28] Y. Seki, H. Funahashi, M. Kitaguchi, M. Hino, Y. Otake, K. Taketani, and H. M. Shimizu, Multilayer neutron interferometer with complete path separation, J. Phys. Soc. Jpn. **79,** 124201 (2010).

[29] M. Hino, M. Kitaguchi, H. Hayashida, S. Tasaki, T. Ebisawa, R. Maruyama, N. Achiwa, and Y. Kawabata, A study on reflectivity limit of neutron supermirror, Nucl. Instrum. Methods Phys. Res., Sect. A **600,** 207 (2009).

[30] N. Yamamoto, M. Kitaguchi, H. M. Shimizu, Y. Seki, and K. Mishima, Development of pulsed neutron interferometer, in *Proceedings of the 3rd J-PARC Symposium (J-PARC2019)* (Physical Society of Japan, Tokyo, 2021), Vol. 011119, pp. 2–5, 10.7566/JPSCP.33.011119.

[31] P. Saggu, T. Mineeva, M. Arif, D. G. Cory, R. Haun, B. Heacock, M. G. Huber, K. Li, J. Nsofini, D. Sarenac, C. B. Shahi, V. Skavysh, W. M. Snow, S. A. Werner, A. R. Young, and D. A. Pushin, Decoupling of a neutron interferometer from temperature gradients, Rev. Sci. Instrum. **87,** 123507 (2016).

[32] S. Nagamiya, Introduction to J-PARC, Prog. Theor. Exp. Phys. **2012,** 1 (2012).

[33] K. Nakajima et al., Materials and life science experimental facility (MLF) at the Japan proton accelerator research complex II: Neutron scattering instruments, Quantum Beam Sci. **1,** 9 (2017).

[34] K. Mishima, T. Ino, K. Sakai, T. Shinohara, K. Hirota, K. Ikeda, H. Sato, Y. Otake, H. Ohmori, S. Muto, N. Higashi, T. Morishima, M. Kitaguch, M. Hino, H. Funahashi, T. Shima, J. I. Suzuki, K. Niita, K. Taketani, Y. Seki, and H. M. Shimizu, Design of neutron beamline for fundamental physics at J-PARC BL05, Nucl. Instrum. Methods Phys. Res., Sect. A **600,** 342 (2009).

[35] K. Mishima, J-PARC neutron beam line (BL05/NOP) for fundamental physics, Hamon **25,** 156 (2015).

[36] M. Kitaguchi, H. Funahashi, T. Nakura, M. Hino, and H. M. Shimizu, Cold-neutron interferometer of the Jamin type, Phys. Rev. A **67,** 033609 (2003).

[37] Y. Seki, Multilayer neutron interferometer with complete path separation, Ph.D. thesis, Kyoto University, 2011, http://hdl.handle.net/2433/142371.

[38] K. Hirota, T. Shinohara, K. Ikeda, K. Mishima, T. Adachi, T. Morishima, S. Satoh, T. Oku, S. Yamada, H. Sasao, J. I. Suzuki, and H. M. Shimizu, Development of a neutron detector based on a position-sensitive photomultiplier, Phys. Chem. Chem. Phys. **7,** 1836 (2005).

[39] See Supplemental Material at http://link.aps.org/supplemental/10.1103/PhysRevLett.132.023402, which includes Refs. [1,40–42], for the derivation of the fitting equation, details of the determination of the experimental values and their uncertainties, and impurity analysis of the measured samples.

[40] S. Sakurai, Industrial users society for neutron application season report Vol. 37, technical report, Taiyo Koko, 2017.

[41] T. Prohaska et al., Standard atomic weights of the elements 2021 (IUPAC Technical Report), J. Macromol. Sci. Part A Pure Appl. Chem. **94,** 573 (2022).

[42] H. Yoshinaga, Recovery of molybdenum and vanadium from spent catalyst, J. MMIJ **123,** 768 (2007).

[43] D. A. Pushin, M. G. Huber, M. Arif, C. B. Shahi, J. Nsofini, C. J. Wood, D. Sarenac, and D. G. Cory, Neutron interferometry at the national institute of standards and technology, Adv. High Energy Phys. **2015,** 1 (2015).

[44] https://j-parc.jp/researcher/MatLife/ja/instrumentation/index.html.

[45] S. Varley F, Neutron scattering lengths and cross sections, Neutron News **3,** 26 (1992).

[46] W. Bauspiess, U. Bonse, and H. Rauch, The prototype neutron interferometer at the Grenoble high flux reactor, Nucl. Instrum. Methods **157,** 495 (1978).

[47] T. Hosobata, N. L. Yamada, M. Hino, Y. Yamagata, T. Kawai, H. Yoshinaga, K. Hori, M. Takeda, S. Takeda, and S.-Y. Morita, Development of precision elliptic neutron-focusing supermirror, Opt. Express **25,** 20012 (2017).

[48] T. Hosobata, N. L. Yamada, M. Hino, H. Yoshinaga, F. Nemoto, K. Hori, T. Kawai, Y. Yamagata, M. Takeda, and S. Takeda, Elliptic neutron-focusing supermirror for illuminating small samples in neutron reflectometry, Opt. Express **27,** 26807 (2019).

[49] M. G. Huber, M. Arif, W. C. Chen, T. R. Gentile, D. S. Hussey, T. C. Black, D. A. Pushin, C. B. Shahi, F. E. Wietfeldt, and L. Yang, Neutron interferometric measurement of the scattering length difference between the triplet and singlet states of n-^{3}He, Phys. Rev. C **90,** 064004 (2014).